JACS Au
AN OPEN ACCESS JOURNAL OF THE AMERICAN CHEMICAL SOCIETY



pubs.acs.org/jacsau
Article

# Multifunctional Supramolecular Gels with Strong Mechanical Properties Formed by Self-Assembly of Polyoxometalate-Based Coordination Polymers

Lorenzo Casimiro, Florence Volatron, Grégoire Boivin, Benjamin Abécassis, Sandra Alves, Dalil Brouri, David Montero, Jean-Michel Guigner, Lise-Marie Chamoreau, Geoffrey Gontard, David Portehault, Yanling Li, Anna Proust, Rodrigue Lescouëzec, Guylaine Ducouret, Albert Solé-Daura,* Patrick Davidson,* Théo Merland,* and Guillaume Izzet*

Cite This: *JACS Au* 2024, 4, 4948−4956

Read Online

ACCESS | Metrics & More | Article Recommendations | Supporting Information

**ABSTRACT:** Metallogels built in a bottom-up approach by metal coordination and supramolecular interactions have important potential for the elaboration of smart materials. In this context, we present here the formation of supramolecular coordination polymers driven by the complexation of cobalt(II) or zinc(II) ions with polyoxometalate-based hybrids displaying two terpyridine ligands in a linear arrangement. Thanks to the electrostatic interactions between the polyoxometalate cores and metal nodes, the polymer chains self-assemble into fibers that physically cross-link to form gels above a critical concentration. Using spectroscopy, microscopy, X-ray scattering, and rheometry, complemented by molecular dynamics simulations, we investigated the supramolecular organization of the chains in the fibers and the resulting processes leading to gelation. Compared to previously reported systems, these gels have improved rheological features and appealing properties, such as birefringence, luminescence, and spin crossover, paving the way for their use as building blocks for multifunctional smart materials.

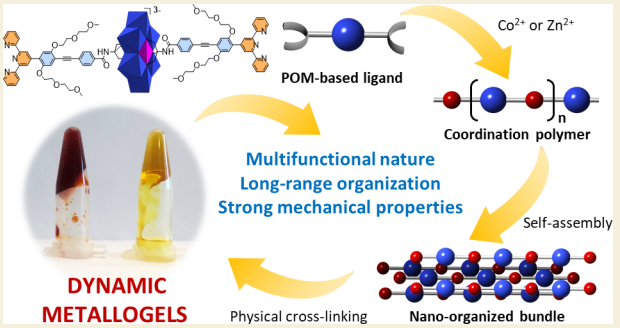


**KEYWORDS:** *metallogels, self-assembly, polyoxometalates, organic−inorganic hybrids, rheology*

## INTRODUCTION

Supramolecular metallogels are a fascinating class of gels, whose formation relies on the use of metal ions as linking agents, assisted by further noncovalent forces (e.g., van der Waals, H-bonds, and $\pi-\pi$ or metal−metal interactions).[1−7] These self-assembled materials can often undergo macro-, micro-, or nanoscopic phase transitions, leading to modulation of the shape, volume, and rheological properties in response to a stimulus.[4,8,9] The presence of metals has been shown to be very beneficial in providing the gels with enhanced properties (e.g., conductive, magnetic, (photo)catalytic, and self-healing) and stimulus responsivity, thus representing a major asset for their application as sensors or smart materials.[1,4,8,10−13] In this regard, current efforts are devoted to incorporating into the building blocks further functional entities to make the system responsive to multiple external stimuli. The gelation mechanism results from the interplay of polymerization by metal coordination and noncovalent interactions between the coordination polymer chains.[4,7] In particular, to induce cross-linking, much care is paid to endow the building blocks with chemical reticulation points (e.g., in branched or multidentate ligands)[14−17] or further complementary moieties (e.g., host−guest pairs),[18,19] in order to exert precise control over the self-assembly and thus build a homogeneous network. Moreover, considerable effort in molecular design and synthesis is required to build systems where the metal is responsible for both coordination and cross-linking.[20−23] To date, the elucidation of the molecular and supramolecular arrangement and of the resulting gelation mechanism using spectroscopy and electron microscopy techniques is usually challenging due to the low electron density of the organic building blocks, so that the gelation mechanism has most often been poorly understood or only hypothesized.[4,24] Furthermore, supramolecular metallogels frequently have limited macroscopic properties, especially in terms of rheology, which remains a

Received: October 18, 2024
Revised: November 12, 2024
Accepted: November 13, 2024
Published: December 5, 2024





https://doi.org/10.1021/jacsau.4c00981
*JACS Au* 2024, 4, 4948−4956

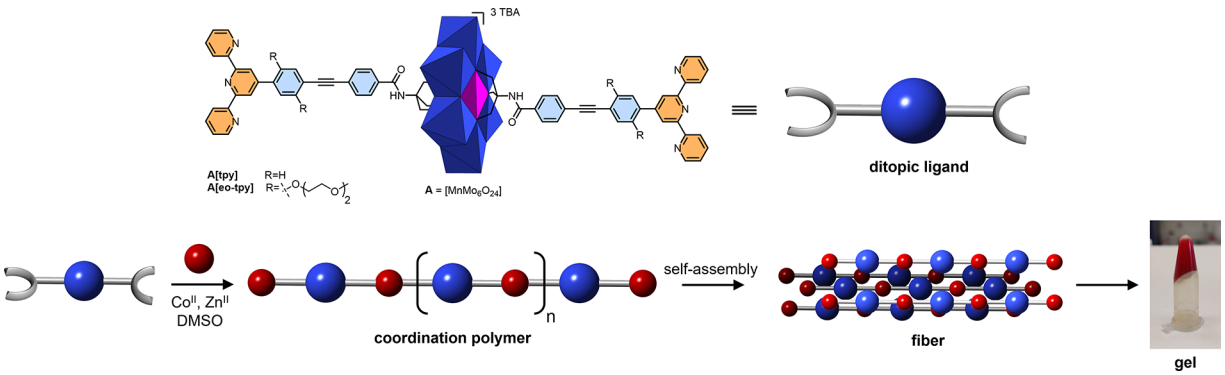


**Figure 1.** Molecular structures of the organic and hybrid compounds and schematic representation of the coordination-driven gelation process (TBA: tetrabutylammonium).

scientific challenge for the development of multifunctional coordination-driven soft materials.[4,5,8,25,26]

In this context, we have previously reported hierarchically self-assembled nanostructures formed by the coordination of metallic ions (e.g., iron, cobalt, and palladium) with organic/inorganic mono- or ditopic hybrids bearing remote terminal (poly)pyridine groups as coordination sites for the metal ions, linked to a polyoxometalate (POM) core.[27−32] POMs are polyanionic metal oxides widely used as inorganic scaffolds due to their rich redox properties and well-defined molecular structure. Furthermore, they can be chemically functionalized into organic−inorganic hybrids[33,34] in which the hybrid compound can not only combine the benefits of the organic and inorganic parts but can also potentially exhibit synergistic properties, which has been the rationale of this growing field. In our previously reported systems, the presence of charged subunits (POM and metal linker) in the self-assembled architectures drove their aggregation, resulting from a competition between the solvation energy of discrete supramolecular species and the intermolecular electrostatic interactions. We then reported the elaboration of discrete metallomacrocycles, nanoparticles, 1D aggregates, and even supramolecular gels, depending on the denticity of the hybrid, the charge of the metal ion, and the dissociating character of the solvent.[27−29] Rare examples of metallogels using hybrid POMs have already been described, but these reports do not mention any salient physicochemical property, probably due to limited mechanical performance or a lack of control over the interactions (gel syneresis was described in one example).[35−37]

We report here a new supramolecular metallogel formed by a covalent organic−inorganic POM-based polymer, extending our previous exploration of POM-based metallogels.[27] The hybrid polymer chains are based on the Anderson POM structure connected through rigid organic spacers to two remote terpyridine units, favoring linear supramolecular polymerization by coordination to divalent metal cations (Figure 1). Metal coordination spontaneously induces the formation of a supramolecular gel above a percolation concentration, ultimately leading to mechanical properties that are considerably improved compared to those usually reported. The presence of an inorganic polymetallic core with a high electron density allowed the use of X-ray scattering and electron microscopy techniques, which provided insights into the internal nano-organization of the material and the nature of the gelation process, also supported by molecular dynamics simulations. These materials exhibit various features, such as optical and magnetic properties, self-healing after mechanical stress, or birefringence, paving the way for high-performance multifunctional materials based on hybrid molecular building blocks.

## RESULTS AND DISCUSSION

### Molecular Design and Synthesis

The synthesis of two new ditopic hybrids, namely, **A**[**tpy**] and **A**[**eo-tpy**] (Figure 1), was developed. These compounds are composed of two terminal terpyridine units, linked to an Anderson polyoxometalate core (**A** = [$MnMo_6O_{24}$]) by rigid aromatic spacers making a 180° angle, a topology prone to favor linear coordination polymers in the presence of divalent metal cations. The hybrids were obtained from the reaction of tetrabutylammonium octamolybdate and manganese acetate with the tris-alkoxide ligands **tris-tpy** and **tris-eo-tpy**, developed from multistep syntheses detailed in Section 2 of the Supporting Information. As **A**[**tpy**] showed limited solubility in various organic solvents, we developed derivative **A**[**eo-tpy**] with ethylene oxide side chains to improve its solubility in organic polar solvents. Single crystals of **A**[**tpy**] and **A**[**eo-tpy**] were grown by the slow diffusion of diethyl ether into acetonitrile solutions of the hybrids. Only single crystals of **A**[**tpy**] were suitable for X-ray structure determination (Figure 2 and SI Section 3), which confirmed

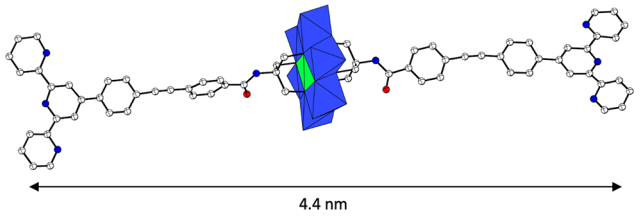


**Figure 2.** X-ray structure of **A**[**tpy**]. H atoms, solvent molecules, and counterions have been omitted for clarity. Mo and Mn polyhedra are colored blue and green, respectively. C, O, and N atoms are shown in white, red, and blue, respectively.

the linear arrangement of the two terpyridine moieties in the hybrid, whose length is 4.4 nm. The unit cell parameters and the space group, $P\bar{1}$, of **A**[**eo-tpy**] could be determined, and it differs from that, $P2_1/c$, of **A**[**tpy**] showing that these compounds have different crystalline structures.

### Metal Complexation

The ability of **A**[**tpy**] to form coordination polymers was surveyed in the presence of 1 equiv of Co(II) in DMSO.



https://doi.org/10.1021/jacsau.4c00981
JACS Au 2024, 4, 4948−4956

Interestingly, a red-colored birefringent metallogel is formed instantaneously (Figure S4.1), but regardless of the initial concentration of the hybrid, severe syneresis was observed upon mechanical stress, precluding further analysis. In contrast, while 1:1 mixtures of a divalent cation and **A**[**eo-tpy**] produced homogeneous solutions at concentrations below ca. 5 mM (3 wt % in DMSO), above this value, immediate gelation was observed (Figure S4.2). The metal coordination of **A**[**eo-tpy**] was probed in dimethyl sulfoxide (DMSO) with Co(II) and Zn(II) salts via UV−vis absorption and luminescence spectroscopy, in diluted conditions (up to 1 mM). The ligand **A**[**eo-tpy**] displays an intense absorption band centered at 360 nm (Figure 3) assigned to a $\pi-\pi^*$

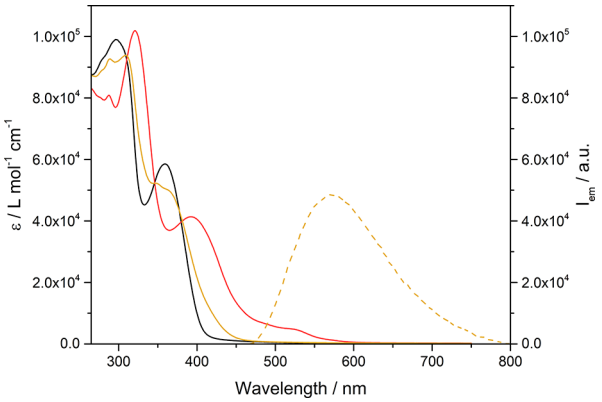


**Figure 3.** UV−vis absorption (full lines) and emission (dashed lines) spectra of **A**[**eo-tpy**] (black), **Co-A**[**eo-tpy**] (red), and **Zn-A**[**eo-tpy**] (yellow) solutions.

transition and a weak and broad absorption band in the visible region attributed to the Mn-Anderson core, which confers it a pale brown color. In the presence of 1 equiv of $[Co(H_2O)_6](NO_3)_2$ or $[Zn(H_2O)_6](BF_4)_2$ salts, the solutions turn red and yellow, respectively, consistently with the formation of $[Co(tpy)_2]^{2+}$ and $[Zn(tpy)_2]^{2+}$ complexes.[38,39] Moreover, the complex **Zn-A**[**eo-tpy**]* showed a weak luminescence ($\Phi_{em}$ < 0.02), with a broad emission band centered at 570 nm whose intensity did not show any time-dependent variation, proving that the coordination is completed within few seconds (Figure S4.3). This emission is considerably weaker and redshifted compared to that of the **tris-eo-tpy** ligand ($\lambda_{em}$ = 452 nm, $\Phi_{em}$ = 0.41) or the **tris-eo-tpy:Zn(II)** complex (2:1) ($\lambda_{em}$ = 469 nm, $\Phi_{em}$ = 0.34, Figure S4.4) as reported in Zn(II) bis-terpyridine molecular materials in the solid state,[40] suggesting the formation of aggregates with **Zn-A**[**eo-tpy**].

The stoichiometry of the metal complexes was further investigated by UV−vis absorption titrations (Figure 4). Upon the addition of increasing aliquots of a concentrated solution of the Co(II) salt to the ligand **tris-eo-tpy** (Figure S4.5), the absorption in the visible region increased up to 0.5 equiv with a shoulder at ca. 520 nm attributed to MLCT and/or d−d transitions,[41] in agreement with the formation of a Co(II) bis-terpyridine complex.[28,42] Beyond this point, any excess of Co(II) ions leads to a slight decrease in absorbance, which may be mainly ascribed to the formation of 1:1 Co-tpy complexes. Titration of the ditopic hybrid **A**[**eo-tpy**] with Co(II) salts resulted in similar absorbance variations, with a maximum absorbance at 1 equiv of Co(II). A similar behavior is observed upon the addition of Zn(II) salt to **tris-eo-tpy** and **A**[**eo-tpy**] (Figure 4 and Figure S4.6.) with the absorbance of the Zn(II)

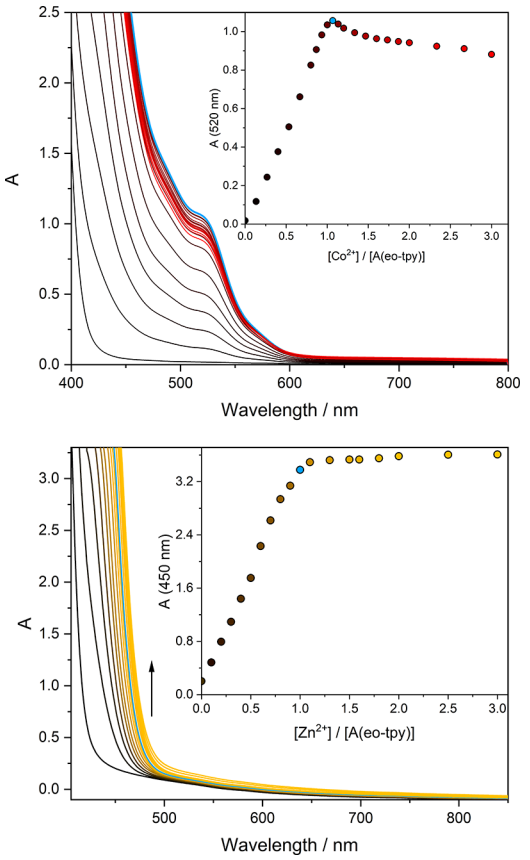


**Figure 4.** UV−vis absorption spectra of a 0.2 mM (top) and 1 mM (bottom) solution of **A**[**eo-tpy**] in DMSO upon the addition of $[Co(H_2O)_6](NO_3)_2$ and $[Zn(H_2O)_6](BF_4)_2$, respectively. The insets show the absorbance changes at 520 and 450 nm, respectively.

bis-terpyridine complex being located more in the UV region compared to Co(II) owing to the absence of MLCT and d−d transitions in this complex.[39] Interestingly, the slope of the absorption evolution upon increasing the Zn(II) content is considerably lower after the addition of 1 equiv of $[Zn(H_2O)_6](BF_4)_2$ to **A**[**eo-tpy**] than after the addition of 0.5 equiv of $[Zn(H_2O)_6](BF_4)_2$ to **tris-eo-tpy**. This suggests that the formation of 1:1 Zn-tpy complexes with **A**[**eo-tpy**] is hindered by a confined environment in the aggregate. These experiments prove that at the equivalent point, all of the terpyridine units of **A**[**eo-tpy**] are bound to the divalent metal center, in line with the formation of coordination polymers. When monitoring the addition of $[Co(H_2O)_6](NO_3)_2$ to a 2 mM solution of **A**[**eo-tpy**] by $^1$H NMR in DMSO-$d_6$, we observed the progressive disappearance of the signals from the terpyridine and ethylene oxide side chains (Figure S4.7). Upon the addition of 0.5 equiv of Co(II), new broad signals at 4.80, 5.86, 6.11, 9.81, 13.2, 31.4, 37.7, and 50.8 ppm are observed, suggesting the intermediate formation of the dimeric **A**[**eo-tpy**]**:Co(II)** (2:1) complex by comparison with the $^1$H NMR signals of an analogue metal bis-terpyridine complex (Figure S4.7).[28] In contrast, upon the addition of 1 equiv of Co(II), no signal is observed from either the free terpyridine or the cobalt bis-terpyridine complex. This is characteristic of colloidal systems, which have a short $T_2$ relaxation time.[43] Similar behavior is observed by $^1$H NMR upon the addition of $[Zn(H_2O)_6](BF_4)_2$ to a 2 mM solution of **A**[**eo-tpy**] (Figure S4.8).



https://doi.org/10.1021/jacsau.4c00981
JACS Au 2024, 4, 4948−4956

## Structural Characterization

To investigate the influence of metal coordination at the supramolecular scale and understand the mechanisms of gel formation, cryo-TEM, TEM, SEM, and small-angle X-ray scattering (SAXS) analyses were undertaken. Cryo-TEM micrographs (Figure 5), recorded on freshly prepared 5 mM

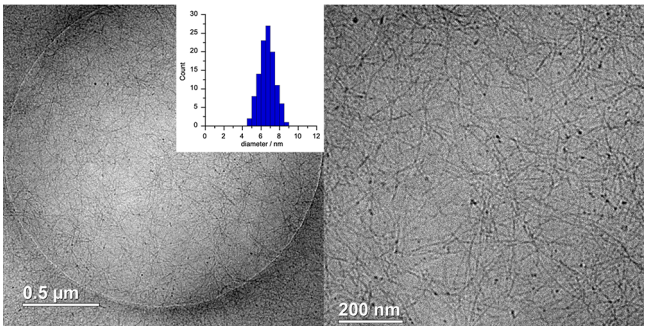


**Figure 5.** Cryo-TEM micrographs of a 5 mM **Co-A[eo-tpy]** gel at different magnifications.

**Co-A[eo-tpy]** (Figure 5) and **Zn-A[eo-tpy]** (Figure S5.1) gels, revealed flexible cylindrical linear objects, with lengths in the range of hundreds of nanometers and respective average diameters of 6.6 and 6.4 nm. These fibers must be bundles of single polymer chains formed by electrostatic interactions between the negative POMs and the positive Co(II) ions, as the Anderson POM has a diameter of ca. 0.9 nm (*vide infra*). As we will show below, the formation of these fibers explains many physical properties of these systems, such as birefringence due to fiber alignment and gelation due to fiber entanglement. SEM (Figure S5.2) and TEM (Figure S5.3) micrographs of 0.1 and 1 mM **Co-A[eo-tpy]** DMSO dropcast solutions also show the presence of monodisperse fibers of similar diameter (ca. 6−7 nm). The fact that the fibers are observed in the dropcast samples could be due to the fact that they are already present in dilute solution. Moreover, the EDS analysis of the samples showed peaks corresponding to all the elements of the material, in particular Mn, Co, and Mo. The quantification by EDS with TEM gave reasonable results. Typically, focusing on a single fiber provided Mn/Co/Mo atomic ratios of 0.81/1.1/6.0, while focusing on a thick film provided Mn/Co/Mo atomic ratios of 0.82/0.85/6.0 (Figure S5.3).

The molecular arrangement of the chains in the fibers of the **Co-A[eo-tpy]** and **Zn-A[eo-tpy]** gels was then studied by SAXS (Figure 6). Regardless of the concentration, the Co and Zn gels showed a main scattering peak at 0.44 and 0.43 $Å^{-1}$, respectively, and their second harmonics at 0.88 and 0.86 $Å^{-1}$ (solid arrows in Figure 6), which are mostly due to the scattering contrast between the POM units and the organic moieties and the solvent. The pronounced asymmetry of the peak, which is striking for **Zn-A[eo-tpy]** but also clear with **Co-A[eo-tpy]**, strongly suggests that it is due to the periodicity of an object with low-dimensionality, as expected here.[44] Indeed, this peak asymmetry (see the inset in Figure 6) is compelling evidence that the diffraction peaks are due to the scattering by the 1D objects observed by cryo-TEM shown in Figure 5. The scattering by 1D chains and the origin of the peak asymmetry have been analyzed in detail by Schlesinger et al.[45] Furthermore, a minimum estimate for the polymer length of 25 and 75 nm for **Co-A[eo-tpy]** and **Zn-A[eo-tpy]**,

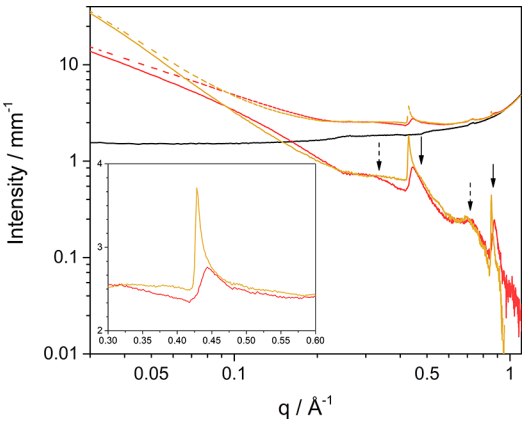


**Figure 6.** SAXS diffractograms of 10 mM gel of **Co-A[eo-tpy]** (dashed red line) and **Zn-A[eo-tpy]** (dashed yellow line), DMSO (black line), and their difference with the solvent (solid red and yellow lines, respectively); the main scattering peak and its first harmonic are indicated by solid arrows, and broader scattering peaks are shown by dashed arrows. The inset shows the peak asymmetry on linear−linear scales.

respectively, can be derived from the full width at half-maximum of the reflections. Note that these minimum values are considerably lower than the length of the fibers actually observed by microscopy techniques. However, the lower bounds of the fibril length, thus roughly estimated from the SAXS reflection profiles, correspond to the size of coherent domains in the fibers, which may indicate that the long fibers are composed of shorter polymeric chains.

This scattering peak corresponds to a period of 1.47 nm, a value that is one-third of the total length of the chain repeat unit (*vide infra*). This implies that the POM units of three first-neighbor chains in a fiber are axially staggered by one-third of the total length of the hybrid monomer (see scheme in Figures 1 and 7). The scattering curve also shows two broad bumps

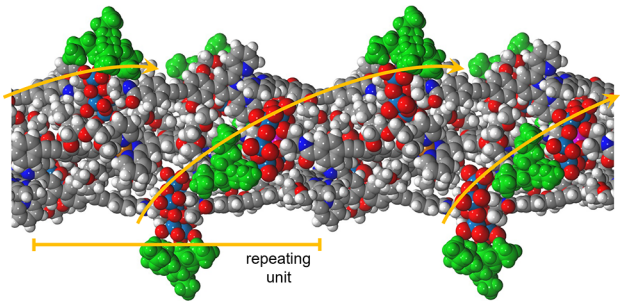


**Figure 7.** Molecular structure of a fiber composed of 5 polymer chains obtained by MD simulations. For clarity reasons, the TBA counterions are shown in green, and the repeating unit and helical pattern are shown in yellow.

around 0.3 and 0.7 $Å^{-1}$ (dashed arrows in Figure 6), which could be related to the packing of the polymer chains in the plane perpendicular to the fibers, but these scattering data are too sparse to draw an exhaustive model. We have also recorded the XRD patterns of dried **Co-A[eo-tpy]** and **Zn-A[eo-tpy]** samples, after precipitation using diethyl ether (Figure S4.9). Interestingly, a strong diffuse scattering peak at 0.47 $Å^{-1}$ (0.46 $Å^{-1}$) and other weaker peaks at 0.72 $Å^{-1}$ (0.71 $Å^{-1}$), 0.94 $Å^{-1}$ (0.89 $Å^{-1}$), 1.19 $Å^{-1}$ (1.16 $Å^{-1}$), and 1.44 $Å^{-1}$ (1.44 $Å^{-1}$) are observed for **Co-A[eo-tpy]** (and **Zn-A[eo-tpy]**, respectively).


https://doi.org/10.1021/jacsau.4c00981
JACS Au 2024, 4, 4948−4956

The peaks at 0.47 $Å^{-1}$ (0.46 $Å^{-1}$) and 0.94 $Å^{-1}$ (0.89 $Å^{-1}$) are close to those already observed by SAXS (note that no peak was found at ca. 0.3 $Å^{-1}$). The peak at 0.72 $Å^{-1}$ (0.71 $Å^{-1}$) with its second harmonics at 1.44 $Å^{-1}$ corresponds to a distance of 0.9 nm, and it could be attributed to some average distance between the chains within the fibers. Finally, the ratio of the positions of the broad peaks at 1.19 $Å^{-1}$ (1.16 $Å^{-1}$) and 0.72 $Å^{-1}$ (0.71 $Å^{-1}$) is ca. 1.65, which is close to $\sqrt{3}$. The observation of this peak suggests local hexagonal packing of the polymeric chains in the bundles.

## Molecular Dynamics Simulations

To gain more insight into the fiber structure, we performed molecular dynamics (MD) simulations on a 3D box containing 5 periodic **Co-A[tpy]** polymer chains embedded in an explicit DMSO solvent and TBA counter cations compensating the charge (see SI Section 6, Figure S6.1). Within 1.1 $\mu$s, the chains aggregated into fibers with interchain distances shorter than 1.5 nm, most commonly at 1.04 nm (Figure S6.2). These aggregates most likely form due to the electrostatic interactions between the negatively charged POM cores and the positively charged metal nodes and to the van der Waals interactions between the ethylene oxide side chains, whereas aggregates with larger interchain distances (1.5−2.5 nm) would form by the intercalation of a TBA counterion between the chains (Figure S6.2−3). The solvent molecules are an important factor in the simulations: when DMSO molecules are included in the calculation, the aggregates form at POM···POM distances of ca. 1.5 nm only in 7% of the samples, most likely due to shielding of the chain−chain contacts by the solvent. Instead, solvent-free simulations were performed (Figure S6.4) and showed a predominant 1.5 nm Mn···Mn distance as observed by SAXS, suggesting that the aggregation process would expel the DMSO molecules, giving rise to a compact structure where the POMs and the metal units interact directly and the POM−POM interactions are mediated by intercalated TBA counterions (Figure 7). These findings are nicely consistent with the SAXS analysis and with the TEM-EDS analysis of the fibers. Moreover, in the dry sample, the most frequent interchain distance was 0.94 nm, in agreement with the value observed by SAXS and P-XRD. This implies that an average fiber of 6.5 nm diameter, as measured by cryo-TEM analysis, would be formed by ca. 40 polymer chains, calculated by dividing the area of the fiber by that of the chains, considering a hexagonal compact packing.

Interestingly, the axial displacement of three consecutive chains by one-third of the total length of the hybrid monomer suggests that the polymer chains in the fibers could be packed in a helical fashion. The helical organization of the POMs in the fibers can indeed be observed in the structure obtained by the simulations. The system might be optically inactive because the fibers are expected to display supramolecular chirality of both signs in equal amounts.[46] Cryo-TEM, SAXS analysis, and MD simulations confirmed that, after complexation of the metal ions, the polymer chains self-assemble into fibers, probably owing to electrostatic interactions, as previously observed in similar POM-based systems[27−29] and to a lesser extent to van der Waals interactions. This suggests that the gelation process is most likely due to a purely physical intertwining of the chains rather than chemical cross-linking at the molecular level.

## Birefringence

At the macroscopic level, supramolecular self-assembly strongly affects the optical and rheological properties of the suspensions. A dilute suspension (e.g., below 5 mM), placed between two crossed polarizer films, appears completely dark, meaning that it is not birefringent (and therefore completely isotropic). However, gentle shaking produces a vivid flow birefringence pattern (Figure S4.10). Such flow birefringence is evidence that the suspension contains anisotropic objects (i.e., the polymer chains or fibers) that are transiently aligned by shear flow, even at a low concentration. The birefringence of the supramolecular gels at a higher concentration, sucked into flat glass optical capillaries immediately after preparation, was studied with a polarizing microscope. All samples showed a pronounced birefringence, although completely uniform samples were challenging to obtain by aspiration in the capillaries (Figure 8 and Figure S4.11).

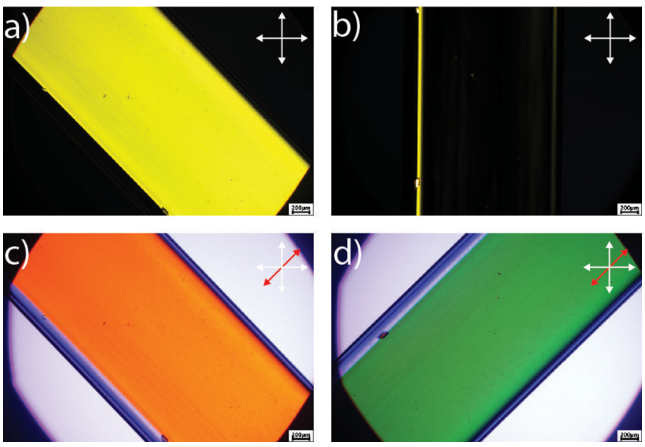


**Figure 8.** Photographs in polarized light microscopy of a (a−d) 10 mM **Co-A[eo-tpy]** metallogel sample sucked into a flat glass capillary of axis at 45° (a) or parallel (b) to the polarizer axes (white cross). (c,d) The use of a wave plate (red arrow) shows that the sample slow axis is parallel to the capillary axis. Note that the usual blue and purple colors shift to green and orange due to the yellow color of the sample.

They are dark when the capillary axis is parallel to one of the polarizer axes and bright when the capillary axis is at 45°. Moreover, adding a wave plate in the microscope light path revealed that the largest refraction index (i.e., the slow axis) is along the capillary main axis. This means that on average, the fibers have aligned along the shear flow that occurred during sample preparation, while the increase in birefringence is most likely due to some improvement in fiber alignment as the gel ages. The birefringence increased slightly over several hours, which suggests that the assembly still grows on this timescale. A further increase was observed upon heating to 100 °C, possibly due to the release of mechanical constraints such as entanglements. The birefringence value, $\Delta n = 6.5 \times 10^{-4}$, measured with an optical compensator, is in line with that of other dilute suspensions of rod-like nanoparticles.[47] The birefringence shows that the polymer chains and their fibers undergo spontaneous cooperative alignment at the macroscopic level, as in a nematic phase.[48]

## Magnetic Properties

Preliminary measurements were performed on dry samples obtained by precipitation of **Co-A[eo-tpy]** and **Zn-A[eo-tpy]** gels in diethyl ether. While the Zn analogue did not show any



https://doi.org/10.1021/jacsau.4c00981
JACS Au 2024, 4, 4948−4956

signal, **Co-A[eo-tpy]** underwent a gradual thermal transition between 100 and 400 K, in line with the typical spin crossover of $[Co(tpy)_2]^{2+}$ complexes[38,49] from a low spin state at low temperatures to a high spin state at high temperatures (Figure 9). The wide temperature range covered by the transition could be related to the occurrence of different local environments for the Co spin crossover centers.

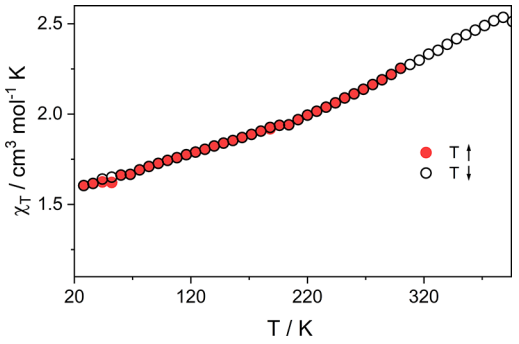


**Figure 9.** Product of the mass susceptibility and the temperature of a dried **Co-A[eo-tpy]** gel in the range of 20−400 K. The analogue **Zn-A[eo-tpy]** dried gel was used to correct for the diamagnetic contribution.

These measurements provide additional evidence that the presence of the metal ion adds value to the material, namely, the ability to undergo spin crossover under thermal stimuli. Further measurements to unravel the magnetic properties of the gels and their correlation with supramolecular organization are currently underway.

## Rheological Properties

The viscoelastic properties of the gels were quantified by dynamic rheological measurements. Freshly prepared **Co-** and **Zn-A[eo-tpy]** gels displayed moderate storage ($G'$, material elastic response) and loss ($G''$, viscous response) moduli (Figure 10 and Figure S7.1), which then gradually increased by more than 1 order of magnitude within 1 day, up to $57 \times 10^3$ and $4.8 \times 10^3$ Pa, respectively.

This means that although complexation is almost instantaneous when **A[eo-tpy]** is mixed with the metal (*vide infra*), the system is still evolving to strengthen the interactions between the fibers in the gel. The long timescale of the self-assembly could be due to the increase in viscosity, which could slow down the diffusion of the fibers. In the literature, metallogels often display much weaker storage moduli of ca. $10^2$−$10^3$ Pa for concentrations of the order of few wt %.[10,11,20,21,50−52] Examples of stiff metallogels with a storage modulus exceeding $10^5$ Pa have seldom been reported, and in these cases, the system required higher gelator concentrations.[18,53,54] Similar stiffening over time was observed for the Zn analogue (Figure S7.1), meaning that there is the same number of associations for both Co and Zn. Stress−strain experiments (Figure 11 and Figure S7.2) with a 1-day-old 10 mM **Co-A[eo-tpy]** gel show that the breaking point occurs at 6% strain, i.e., 10 times lower than for a fresh gel, but it corresponds to a maximal stress equal to 4.5 kPa, which is 4 times higher than for the fresh gel.

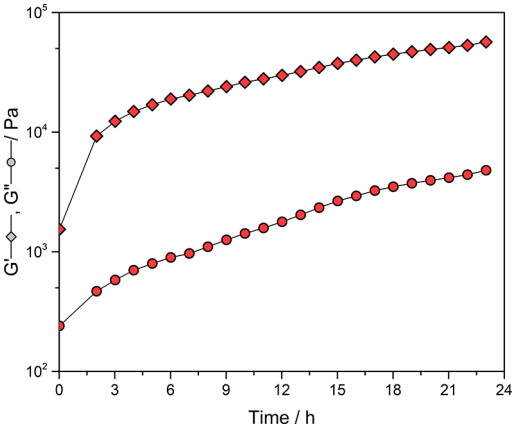


**Figure 10.** Time evolution of the storage (diamonds) and loss (circles) moduli of a 10 mM **Co-A[eo-tpy]** sample. Experimental conditions: strain, 0.5%; frequency, 1 Hz; 25 °C.

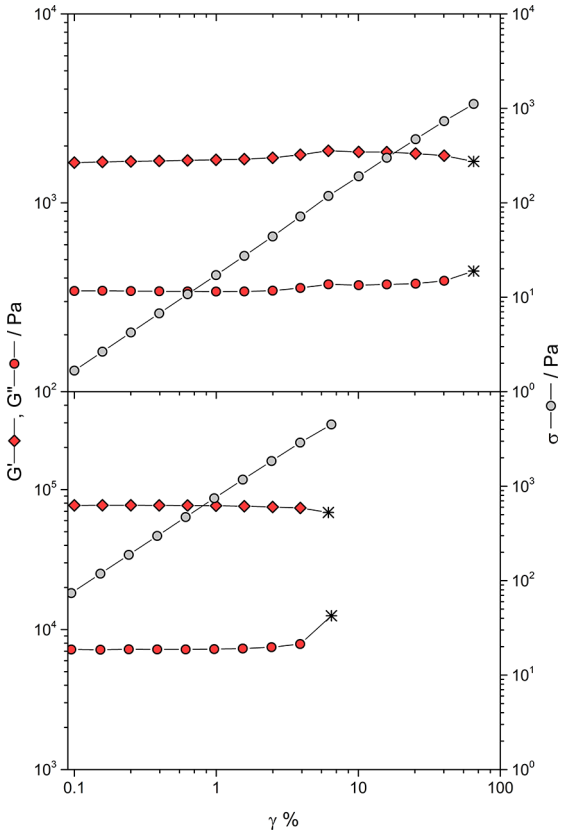


**Figure 11.** Storage (red diamonds) and loss (red circles) moduli and stress ($\sigma$, gray circles) versus strain $\gamma$ for a fresh (top) and a 1-day-aged (bottom) 10 mM **Co-A[eo-tpy]** gel. Experimental conditions: frequency = 1 Hz, 25 °C, and strain going from 0.1 to 100%.

Fatigue resistance experiments were performed on the aged Co(II) gel by imparting 5 cycles of fracture at a strain beyond the breaking point followed by recovery (Figure 12 and Table S7.1). After the first cycle, the storage modulus decreased by half its value and partially recovered from it, which is similar to other systems reported in the literature that are, however, much weaker.[10,11] The four other cycles of fracture only led to a minor decrease in moduli (Table S6.1). Interestingly, recovery occurs again within seconds after decreasing the strain, but the prolonged exposure to high strain compared to stress−strain experiments (Figure 11) leads to a partial loss of the mechanical properties. The latter indicates that the network does not lie on the metal-terpyridine coordination


https://doi.org/10.1021/jacsau.4c00981
JACS Au 2024, 4, 4948−4956

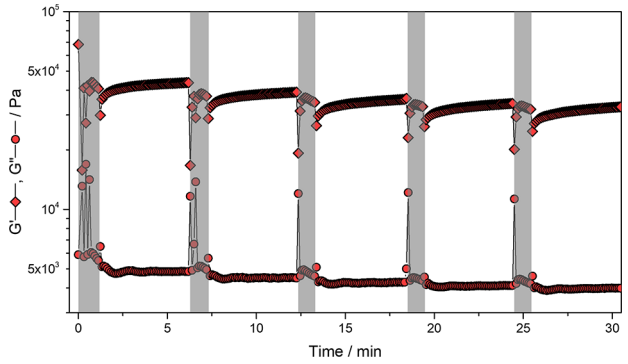


**Figure 12.** Fatigue test of the storage (diamonds) and loss (circles) moduli of a 10 mM **Co-A[eo-tpy]** metallogel during successive cycles of 25% strain followed by 0.1% strain. Experimental conditions: frequency, 1 Hz; 25 °C.

that would easily rebuild but rather on the interactions between the coordination polymer chains.

Overall, these measurements highlight that including a POM-based inorganic core in the molecular design imparts the metallogel with remarkable rheological properties, as high stiffness can be achieved even at a low gelator concentration. Moreover, it confers to the material the ability to stand stresses up to the kPa scale while displaying appealing self-healing properties.

## CONCLUSIONS

We synthesized Anderson-type POM hybrids bearing two remote terpyridine groups. The complexation of cobalt(II) and zinc(II) ions by these molecular hybrids, owing to the linear arrangement of the ditopic terpyridine ligands, induces the formation of rigid linear polymer chains (with a POM and a metal complex in each repeating unit). Furthermore, polyanionic POMs act as negatively charged sites in the coordination polymer. The oppositely charged species (polyanionic POMs and cationic metal complexes) most probably experience attractive electrostatic interactions leading to the formation of bundles (as shown by numerical simulations) and to supramolecular gels above a critical concentration. Improved solubility and stability of the POM hybrids were achieved by grafting oligo(ethylene oxide) units onto the spacers. The presence of the polymetallic core with a high electron density allowed the use of X-ray scattering and electron microscopy techniques, which provided insight into the internal supramolecular organization of the material and the nature of the gelation process. At the macroscopic level, the gels display original optical and rheological properties, such as the spontaneous alignment of the polymer chains, giving rise to birefringence and outstanding rheological performance. To the best of our knowledge, such combined appealing features have never been reported for metallogels. The redox activity of both the coordination complex and the POM scaffolds opens perspectives for the development of multiresponsive metallogels as smart materials.

## ASSOCIATED CONTENT

### Supporting Information

The Supporting Information is available free of charge at https://pubs.acs.org/doi/10.1021/jacsau.4c00981.

Synthesis protocols, NMR spectra for all compounds, and mass spectrometry spectra of the POM-based hybrids; additional experimental details, materials, and methods, including UV−vis and emission spectra, P-XRD, electron microscopy, photographs of the gels, polarized light microscopy, molecular dynamics simulations, and rheology (PDF)

Crystallographic information for **A[tpy]** (CIF)

## AUTHOR INFORMATION


### Corresponding Authors

**Albert Solé-Daura** − *Department de Química Física i Inorgànica, Universitat Rovira i Virgili, Tarragona 43007, Spain;* Present Address: Institute of Chemical Research of Catalonia (ICIQ-CERCA), The Barcelona Institute of Science and Technology, 43007 Tarragona, Spain; orcid.org/0000-0002-3781-3107; Email: albert.soled@urv.cat

**Patrick Davidson** − *Université Paris-Saclay, CNRS, Laboratoire de Physique des Solides, 91405 Orsay, France*; Email: patrick.davidson@universite-paris-saclay.fr

**Théo Merland** − *Laboratoire Science et Ingénierie de la Matière Molle, SIMM, Sorbonne University, ESPCI Paris, CNRS, PSL University, Paris F-75005, France*; Email: theo.merland@espci.psl.eu

**Guillaume Izzet** − *Sorbonne Université, CNRS, Institut Parisien de Chimie Moléculaire, IPCM, F-75005 Paris, France;* orcid.org/0000-0002-9849-4939; Email: guillaume.izzet@sorbonne-universite.fr

### Authors

**Lorenzo Casimiro** − *Sorbonne Université, CNRS, Institut Parisien de Chimie Moléculaire, IPCM, F-75005 Paris, France;* orcid.org/0000-0002-8818-5913

**Florence Volatron** − *Sorbonne Université, CNRS, Institut Parisien de Chimie Moléculaire, IPCM, F-75005 Paris, France;* orcid.org/0000-0002-1009-0412

**Grégoire Boivin** − *Sorbonne Université, CNRS, Institut Parisien de Chimie Moléculaire, IPCM, F-75005 Paris, France*

**Benjamin Abécassis** − *CNRS, ENS de Lyon, LCH, UMR 5182, 69342 Lyon, France;* orcid.org/0000-0002-1629-9671

**Sandra Alves** − *Sorbonne Université, CNRS, Institut Parisien de Chimie Moléculaire, IPCM, F-75005 Paris, France*

**Dalil Brouri** − *Sorbonne Université, CNRS, Laboratoire de Réactivité de Surface, LRS, F-75005 Paris, France*

**David Montero** − *Sorbonne Université, CNRS, Fédération de Chimie et Matériaux de Paris-Centre, Paris F-75005, France*

**Jean-Michel Guigner** − *Sorbonne Université, CNRS, Muséum National d'Histoire Naturelle, Institut de Minéralogie, de Physique des Matériaux et de Cosmochimie, IMPMC, F-75005 Paris, France*

**Lise-Marie Chamoreau** − *Sorbonne Université, CNRS, Institut Parisien de Chimie Moléculaire, IPCM, F-75005 Paris, France*

**Geoffrey Gontard** − *Sorbonne Université, CNRS, Institut Parisien de Chimie Moléculaire, IPCM, F-75005 Paris, France;* orcid.org/0000-0002-4099-5423

**David Portehault** − *Sorbonne Université, CNRS, Laboratoire de Chimie de la Matière Condensée de Paris, LCMCP, F-75005 Paris, France;* orcid.org/0000-0003-4914-4913




https://doi.org/10.1021/jacsau.4c00981
JACS Au 2024, 4, 4948−4956

**Yanling Li** − *Sorbonne Université, CNRS, Institut Parisien de Chimie Moléculaire, IPCM, F-75005 Paris, France*
**Anna Proust** − *Sorbonne Université, CNRS, Institut Parisien de Chimie Moléculaire, IPCM, F-75005 Paris, France;* orcid.org/0000-0002-0903-6507
**Rodrigue Lescouëzec** − *Sorbonne Université, CNRS, Institut Parisien de Chimie Moléculaire, IPCM, F-75005 Paris, France;* orcid.org/0000-0003-3510-5112
**Guylaine Ducouret** − *Laboratoire Science et Ingénierie de la Matière Molle, SIMM, Sorbonne University, ESPCI Paris, CNRS, PSL University, Paris F-75005, France*

Complete contact information is available at: https://pubs.acs.org/10.1021/jacsau.4c00981

### Author Contributions

The manuscript was written through contributions of all authors.

### Funding

This project has received financial support from the CNRS through the MITI interdisciplinary programs. L.C. acknowledges the Initiative pour les Sciences et l'Ingénierie Moléculaires (iSiM) de l'Alliance Sorbonne Université for funding his postdoctoral fellowship. A.S.-D. acknowledges the Spanish Ministry of Universities and the European Union-Next Generation EU for their financial support through a Margarita Salas grant.

### Notes

The authors declare no competing financial interest.

## ■ ACKNOWLEDGMENTS

The authors gratefully acknowledge SOLEIL for provision of synchrotron radiation facilities (under the approved proposal no. 20221057). We thank Thomas Bizien and Stéphan Rouzière for help with the X-ray scattering experiments (SOLEIL and tests at MORPHEUS Platform of LPS, respectively). The XRD facility of IMPMC is acknowledged for the recording of powder diffraction patterns of gels and for their help in these measurements. SEM & EDS were funded by Sorbonne Université, CNRS and Région Ile de France, and are part of FCMat, The Federation of Chemistry and Materials of Paris-Center. We also acknowledge Dr. Cédric Lorthioir and Dr. Matthieu Raynal for fruitful discussions and help in the experimental analyses and Romerson Palad for the synthesis of **A**[**tpy**].

## ■ ADDITIONAL NOTE

[*]**Zn-A**[**eo-tpy**] and **Co-A**[**eo-tpy**] respectively refer to the **A**[**eo-tpy**]:Zn(II) and **A**[**eo-tpy**]:Co(II) complexes with a 1:1 stoichiometry.

## ■ REFERENCES

(1) Piepenbrock, M.-O. M.; Lloyd, G. O.; Clarke, N.; Steed, J. W. Metal- and Anion-Binding Supramolecular Gels. *Chem. Rev.* **2010**, *110* (4), 1960−2004.
(2) Tam, A. Y.-Y.; Yam, V. W.-W. Recent Advances in Metallogels. *Chem. Soc. Rev.* **2013**, *42* (4), 1540−1567.
(3) Zhang, J.; Su, C.-Y. Metal-Organic Gels: From Discrete Metallogelators to Coordination Polymers. *Coord. Chem. Rev.* **2013**, *257* (7), 1373−1408.
(4) Liu, Z.; Zhao, X.; Chu, Q.; Feng, Y. Recent Advances in Stimuli-Responsive Metallogels. *Molecules* **2023**, *28* (5), 2274.
(5) Häring, M.; Díaz, D. D. Supramolecular Metallogels with Bulk Self-Healing Properties Prepared by in Situ Metal Complexation. *Chem. Commun.* **2016**, *52* (89), 13068−13081.
(6) Steed, J. W. Anion-Tuned Supramolecular Gels: A Natural Evolution from Urea Supramolecular Chemistry. *Chem. Soc. Rev.* **2010**, *39* (10), 3686−3699.
(7) Fages, F. Metal Coordination To Assist Molecular Gelation. *Angew. Chem., Int. Ed.* **2006**, *45* (11), 1680−1682.
(8) Sutar, P.; Maji, T. K. Recent Advances in Coordination-Driven Polymeric Gel Materials: Design and Applications. *Dalton Trans.* **2020**, *49* (23), 7658−7672.
(9) Steed, J. W. Supramolecular Gel Chemistry: Developments over the Last Decade. *Chem. Commun.* **2011**, *47* (5), 1379−1383.
(10) Adhikary, A.; Das, K. S.; Saha, S.; Roy, M.; Mondal, R. A Free-Standing, Self-Healing Multi-Stimuli Responsive Gel Showing Cryogenic Magnetic Cooling. *Dalton Trans.* **2020**, *49* (38), 13487−13495.
(11) Saha, E.; Karthick, K.; Kundu, S.; Mitra, J. Electrocatalytic Oxygen Evolution in Acidic and Alkaline Media by a Multistimuli-Responsive Cobalt(II) Organogel. *ACS Sustainable Chem. Eng.* **2019**, *7* (19), 16094−16102.
(12) Verma, P.; Singh, A.; Rahimi, F. A.; Sarkar, P.; Nath, S.; Pati, S. K.; Maji, T. K. Charge-Transfer Regulated Visible Light Driven Photocatalytic H2 Production and CO2 Reduction in Tetrathiafulvalene Based Coordination Polymer Gel. *Nat. Commun.* **2021**, *12* (1), 7313.
(13) Verma, P.; Rahimi, F. A.; Samanta, D.; Kundu, A.; Dasgupta, J.; Maji, T. K. Visible-Light-Driven Photocatalytic CO2 Reduction to CO/CH4 Using a Metal−Organic "Soft" Coordination Polymer Gel. *Angew. Chem., Int. Ed.* **2022**, *61* (16), No. e202116094.
(14) Jiang, Z.; Wu, T.; Wu, S.; Yuan, J.; Zhang, Z.; Xie, T.-Z.; Liu, H.; Peng, Y.; Li, Y.; Dong, S.; Wang, P. Self-Healing and Elastic Polymer Gel via Terpyridine-Metal Coordination. *Inorg. Chem. Commun.* **2022**, *146*, No. 110131.
(15) Sun, Z.; Lv, F.; Cao, L.; Liu, L.; Zhang, Y.; Lu, Z. Multistimuli-Responsive, Moldable Supramolecular Hydrogels Cross-Linked by Ultrafast Complexation of Metal Ions and Biopolymers. *Angew. Chem., Int. Ed.* **2015**, *54* (27), 7944−7948.
(16) Chen, P.; Li, Q.; Grindy, S.; Holten-Andersen, N. White-Light-Emitting Lanthanide Metallogels with Tunable Luminescence and Reversible Stimuli-Responsive Properties. *J. Am. Chem. Soc.* **2015**, *137* (36), 11590−11593.
(17) Sutar, P.; Maji, T. K. Coordination Polymer Gels with Modular Nanomorphologies, Tunable Emissions, and Stimuli-Responsive Behavior Based on an Amphiphilic Tripodal Gelator. *Inorg. Chem.* **2017**, *56* (16), 9417−9425.
(18) Lu, C.; Zhang, M.; Tang, D.; Yan, X.; Zhang, Z.; Zhou, Z.; Song, B.; Wang, H.; Li, X.; Yin, S.; Sepehrpour, H.; Stang, P. J. Fluorescent Metallacage-Core Supramolecular Polymer Gel Formed by Orthogonal Metal Coordination and Host−Guest Interactions. *J. Am. Chem. Soc.* **2018**, *140* (24), 7674−7680.
(19) Liu, Y.; Shangguan, L.; Wang, H.; Xia, D.; Shi, B. A Supramolecular Polymer Network Gel with Stimuli-Responsiveness Constructed by Orthogonal Metal Ion Coordination and Pillar[5]-Arene-Based Host−Guest Recognition. *Polym. Chem.* **2017**, *8* (25), 3783−3787.
(20) Gasnier, A.; Royal, G.; Terech, P. Metallo-Supramolecular Gels Based on a Multitopic Cyclam Bis-Terpyridine Platform. *Langmuir* **2009**, *25* (15), 8751−8762.
(21) Gasnier, A.; Bucher, C.; Moutet, J.; Royal, G.; Saint-Aman, E.; Terech, P. Redox-Responsive Metallo-Supramolecular Polymers and Gels Containing bis-Terpyridine Appended Cyclam Ligand. *Macromol. Symp.* **2011**, *304* (1), 87−92.
(22) Terech, P.; Yan, M.; Maréchal, M.; Royal, G.; Galvez, J.; Velu, S. K. P. Characterization of Strain Recovery and "Self-Healing" in a Self-Assembled Metallo-Gel. *Phys. Chem. Chem. Phys.* **2013**, *15* (19), 7338−7344.
(23) Yu, X.; Wang, Z.; Li, Y.; Geng, L.; Ren, J.; Feng, G. Fluorescent and Electrochemical Supramolecular Coordination Polymer Hydro-

gels Formed from Ion-Tuned Self-Assembly of Small Bis-Terpyridine Monomer. *Inorg. Chem.* **2017**, *56* (13), 7512−7518.
(24) Panja, S.; Adams, D. J. Stimuli Responsive Dynamic Transformations in Supramolecular Gels. *Chem. Soc. Rev.* **2021**, *50* (8), 5165−5200.
(25) Wu, H.; Zheng, J.; Kjøniksen, A.-L.; Wang, W.; Zhang, Y.; Ma, J. Metallogels: Availability, Applicability, and Advanceability. *Adv. Mater.* **2019**, *31* (12), No. 1806204.
(26) Datta, S.; Saha, M. L.; Stang, P. J. Hierarchical Assemblies of Supramolecular Coordination Complexes. *Acc. Chem. Res.* **2018**, *51* (9), 2047−2063.
(27) Centellas, M. S.; Piot, M.; Salles, R.; Proust, A.; Tortech, L.; Brouri, D.; Hupin, S.; Abécassis, B.; Landy, D.; Bo, C.; Izzet, G. Exploring the Self-Assembly of Dumbbell-Shaped Polyoxometalate Hybrids, from Molecular Building Units to Nanostructured Soft Materials. *Chem. Sci.* **2020**, *11* (40), 11072−11080.
(28) Piot, M.; Abécassis, B.; Brouri, D.; Troufflard, C.; Proust, A.; Izzet, G. Control of the Hierarchical Self-Assembly of Polyoxometalate-Based Metallomacrocycles by Redox Trigger and Solvent Composition. *Proc. Natl. Acad. Sci. U.S.A.* **2018**, *115* (36), 8895−8900.
(29) Izzet, G.; Abécassis, B.; Brouri, D.; Piot, M.; Matt, B.; Serapian, S. A.; Bo, C.; Proust, A. Hierarchical Self-Assembly of Polyoxometalate-Based Hybrids Driven by Metal Coordination and Electrostatic Interactions: From Discrete Supramolecular Species to Dense Monodisperse Nanoparticles. *J. Am. Chem. Soc.* **2016**, *138* (15), 5093−5099.
(30) Izzet, G.; Macdonell, A.; Rinfray, C.; Piot, M.; Renaudineau, S.; Derat, E.; Abécassis, B.; Afonso, C.; Proust, A. Metal-Directed Self-Assembly of a Polyoxometalate-Based Molecular Triangle: Using Powerful Analytical Tools to Probe the Chemical Structure of Complex Supramolecular Assemblies. *Chem. - Eur. J.* **2015**, *21* (52), 19010−19015.
(31) Piot, M.; Hupin, S.; Lavanant, H.; Afonso, C.; Bouteiller, L.; Proust, A.; Izzet, G. Charge Effect on the Formation of Polyoxometalate-Based Supramolecular Polygons Driven by Metal Coordination. *Inorg. Chem.* **2017**, *56* (14), 8490−8496.
(32) Salles, R.; Abécassis, B.; Derat, E.; Brouri, D.; Bernard, A.; Zhang, Q.; Proust, A.; Desmarets, C.; Izzet, G. Hierarchical Self-Assembly of Polyoxometalate-Based Organo Palladium(II) Metallomacrocycles via Electrostatic Interactions. *Inorg. Chem.* **2020**, *59* (4), 2458−2463.
(33) Proust, A.; Matt, B.; Villanneau, R.; Guillemot, G.; Gouzerh, P.; Izzet, G. Functionalization and Post-Functionalization: A Step towards Polyoxometalate-Based Materials. *Chem. Soc. Rev.* **2012**, *41* (22), 7605.
(34) Anyushin, A. V.; Kondinski, A.; Parac-Vogt, T. N. Hybrid Polyoxometalates as Post-Functionalization Platforms: From Fundamentals to Emerging Applications. *Chem. Soc. Rev.* **2020**, *49* (2), 382−432.
(35) Abhervé, A.; Palacios-Corella, M.; Clemente-Juan, J. M.; Marx, R.; Neugebauer, P.; van Slageren, J.; Clemente-León, M.; Coronado, E. Bimetallic MnIII−FeII Hybrid Complexes Formed by a Functionalized MnIII Anderson Polyoxometalate Coordinated to FeII: Observation of a Field-Induced Slow Relaxation of Magnetization in the MnIII Centres and a Photoinduced Spin-Crossover in the FeII Centres. *J. Mater. Chem. C* **2015**, *3* (30), 7936−7945.
(36) Favette, S.; Hasenknopf, B.; Vaissermann, J.; Gouzerh, P.; Roux, C. Assembly of a Polyoxometalate into an Anisotropic Gel. *Chem. Commun.* **2003**, *21*, 2664−2665.
(37) Yan, J.; Huang, H.; Miao, Z.; Zhang, Q.; Yan, Y. Polyoxometalate-Based Hybrid Supramolecular Polymer via Orthogonal Metal Coordination and Reversible Photo-Cross-Linking. *Macromolecules* **2019**, *52* (24), 9545−9554.
(38) Enachescu, C.; Krivokapic, I.; Zerara, M.; Real, J. A.; Amstutz, N.; Hauser, A. Optical Investigation of Spin-Crossover in Cobalt(II) Bis-Terpy Complexes. *Inorg. Chim. Acta* **2007**, *360* (13), 3945−3950.
(39) Albano, G.; Balzani, V.; Constable, E. C.; Maestri, M.; Smith, D. R. Photoinduced Processes in 4′-(9-Anthryl)-2,2′:6′,2″-Terpyridine, Its Protonated Forms and Zn(II), Ru(II) and Os(II) Complexes. *Inorg. Chim. Acta* **1998**, *277* (2), 225−231.
(40) Winter, A.; Friebe, C.; Chiper, M.; Hager, M. D.; Schubert, U. S. Self-Assembly of π-Conjugated Bis(Terpyridine) Ligands with Zinc(II) Ions: New Metallosupramolecular Materials for Optoelectronic Applications. *J. Polym. Sci., Part A: Polym. Chem.* **2009**, *47* (16), 4083−4098.
(41) Kremer, S.; Henke, W.; Reinen, D. High-Spin-Low-Spin Equilibriums of Cobalt(2+) in the Terpyridine Complexes Co(Terpy)2 × 2.nH2O. *Inorg. Chem.* **1982**, *21* (8), 3013−3022.
(42) Aribia, K. B.; Moehl, T.; Zakeeruddin, S. M.; Grätzel, M. Tridentate Cobalt Complexes as Alternative Redox Couples for High-Efficiency Dye-Sensitized Solar Cells. *Chem. Sci.* **2013**, *4* (1), 454−459.
(43) Osborne, E. A.; Jarrett, B. R.; Tu, C.; Louie, A. Y. Modulation of T2 Relaxation Time by Light-Induced, Reversible Aggregation of Magnetic Nanoparticles. *J. Am. Chem. Soc.* **2010**, *132* (17), 5934−5935.
(44) Warren, B. E. X-Ray Diffraction in Random Layer Lattices. *Phys. Rev.* **1941**, *59* (9), 693−698.
(45) Chen, C.-E.; Schlesinger, Y.; Heeger, A. J. X-Ray Scattering by One-Dimensional Chains: Powder Diffraction. *Phys. Rev. B* **1982**, *25* (4), 2472−2476.
(46) Nadimetla, D. N.; Al Kobaisi, M.; Bugde, S. T.; Bhosale, S. V. Tuning Achiral to Chiral Supramolecular Helical Superstructures. *Chem. Rec.* **2020**, *20* (8), 793−819.
(47) Paineau, E.; Krapf, M.-E. M.; Amara, M.-S.; Matskova, N. V.; Dozov, I.; Rouzière, S.; Thill, A.; Launois, P.; Davidson, P. A Liquid-Crystalline Hexagonal Columnar Phase in Highly-Dilute Suspensions of Imogolite Nanotubes. *Nat. Commun.* **2016**, *7* (1), 10271.
(48) Commeinhes, X.; Davidson, P.; Bourgaux, C.; Livage, J. Orientation of Liquid-Crystalline Suspensions of Vanadium Pentoxide Ribbons by a Magnetic Field. *Adv. Mater.* **1997**, *9* (11), 900−903.
(49) Hayami, S.; Komatsu, Y.; Shimizu, T.; Kamihata, H.; Lee, Y. H. Spin-Crossover in Cobalt(II) Compounds Containing Terpyridine and Its Derivatives. *Coord. Chem. Rev.* **2011**, *255* (17), 1981−1990.
(50) Fang, W.; Sun, Z.; Tu, T. Novel Supramolecular Thixotropic Metallohydrogels Consisting of Rare Metal−Organic Nanoparticles: Synthesis, Characterization, and Mechanism of Aggregation. *J. Phys. Chem. C* **2013**, *117* (47), 25185−25194.
(51) McCarney, E. P.; Byrne, J. P.; Twamley, B.; Martínez-Calvo, M.; Ryan, G.; Möbius, M. E.; Gunnlaugsson, T. Self-Assembly Formation of a Healable Lanthanide Luminescent Supramolecular Metallogel from 2,6-Bis(1,2,3-Triazol-4-Yl)Pyridine (Btp) Ligands. *Chem. Commun.* **2015**, *51* (74), 14123−14126.
(52) Peng, P.; Li, Y.; Song, W.; Yu, X. Self-Healing Organogels and Hydrogels Constructed by Self-Assembled Bis-Terpyridine Complex with Selective Metal Ions. *Colloids Surf.* **2020**, *589*, No. 124439.
(53) Feldner, T.; Häring, M.; Saha, S.; Esquena, J.; Banerjee, R.; Díaz, D. D. Supramolecular Metallogel That Imparts Self-Healing Properties to Other Gel Networks. *Chem. Mater.* **2016**, *28* (9), 3210−3217.
(54) Saha, S.; Bachl, J.; Kundu, T.; Díaz Díaz, D.; Banerjee, R. Amino Acid-Based Multiresponsive Low-Molecular Weight Metallohydrogels with Load-Bearing and Rapid Self-Healing Abilities. *Chem. Commun.* **2014**, *50* (23), 3004−3006.


https://doi.org/10.1021/jacsau.4c00981
*JACS Au* 2024, 4, 4948−4956